Int. J. Heat Mass Transfer. Vol. 37, No. 1, pp. 81–90, 1994
Printed in Great Britain

0017–9310/94 $6.00 + 0.00

A density-weighted reacting model for multi-phase turbulent diffusion flames

S. H. CHAN and M. M. M. ABOU-ELLAIL
Department of Mechanical Engineering, University of Wisconsin–Milwaukee, P.O. Box 784, Milwaukee, WI 53201, U.S.A.

(*Received* 25 *November* 1992 *and in final form* 12 *June* 1993)

Abstract—A reacting multi-fluid model, based on the Favre-averaged separate transport equations for reacting gas–liquid 'multi-phase' flow, is presented. New density-weighted (Favre-averaged) separate transport equations for multi-phase mixture fraction $\tilde{f}$ and its variance g are derived. The new multi-fluid transport equations for $\tilde{f}$ and g are equally applicable to spray flames as well as liquid metal fuel combustors. The fuel spray is discretized into a number of size groups; each group is considered as a separate 'fluid' or 'phase'. A pdf approach, to the reaction process, is adopted. An evaporation variable e is introduced, which is a measure of a nonequilibrium phase state, defining a two-variable pdf as a function of f and e. The instantaneous thermo-chemical properties are computed from a nonequilibrium model. The predicted results, using the present density-weighted multi-fluid model, for an airblast kerosene spray flame are compared with corresponding experimental data. The present multi-fluid model results are in good agreement with the corresponding experimental data for the whole spray flame length.

INTRODUCTION

TURBULENT reacting two-phase flows occur in many engineering applications. Two-phase flames in diesel engine and gas turbine combustion chambers, oil-fired boilers, and liquid metal fuel combustors are some examples. However, due to the complexity in modeling phase-to-phase interaction, two-phase reacting flows have received much less attention than the corresponding single-phase flow system [1–3]. During the last decade, the locally homogeneous flow (LHF) model has been used, with varying degree of success, to predict spray evaporation, spray flames [4], and liquid metal fuel combustors [3, 5–9]. However, interfacial effects and effects of droplet size in spray flames or bubble/droplet size in liquid metal fuel combustors cannot be considered in an LHF model of combustion.

On the other hand, a multi-fluid model can appropriately accommodate the effect of the slip velocity between the phases, droplet/bubble size and difference in turbulent diffusivities of the phases [10]. The two-fluid model, which is a special case of the multi-fluid model, has been used successfully to predict non-reacting and reacting turbulent two-phase flows [10–13]. The multi-fluid model is essentially equivalent to the stochastic separated-flow model when a large number of trajectories are considered for an initially nonuniform droplet-size spray [14, 15].

Recently, the LHF/single-fluid k–ε/single-fluid $\tilde{f}$–g model [16] was used for the prediction of multiphase submerged reacting plumes [7, 8]. In comparison with the recent experimental data [17], it became clear that the existing LHF model is inadequate as it underpredicts the plume length [7]. For this reason, a new multi-phase turbulent reacting model is hereby presented which is expected to be applicable to both the submerged and nonsubmerged reacting flows. Also, new transport equations for $\tilde{f}$ and g of multi-phase reacting flow based on separate transport equations of each phase are presented. Due to the lack of detailed flame structure data for submerged plumes, the developed multi-fluid model is validated by predicting a turbulent co-flowing kerosene spray flame for which detailed experimental data are available [18].

THE PHYSICAL MODEL

The main modeling assumptions and governing equations are presented here. The number of 'fluids' is taken to be $1 + K_d$, where K_d is the number of droplet size groups.

Density-weighted mean flow equations

In the present reacting multi-fluid model, separate transport equations are formulated for each phase (fluid), and the interaction between the phases is accounted for by including interfacial drag and mass exchange source terms resulting from evaporation and mass transfer from one size group to the other. Many terms involving density fluctuations can be avoided by the use of density-weighted variables. For compactness, all the density-averaged, steady state, conservation equations for mass and momentum may be expressed in Cartesian tensor notation although they are actually solved in their cylindrical polar form. The resulting mass conservation equations for the gas

NOMENCLATURE

B transfer number
C_1, C_2, C_3, C_μ multi-phase k–ε model constants
C_{g1}, C_{g2} multi-phase g equation constants
C_p constant-pressure specific heat
d diameter of injector
D droplet diameter
D^k mean droplet diameter of the kth size group
e evaporation variable
f multi-phase mixture fraction (injector fluid mass fraction)
f_1 liquid mixture ratio
g variance of mixture fraction
g_j j-component of the acceleration of gravity
G generation term of turbulence kinetic energy
k turbulence kinetic energy
k_d total number of droplet-size groups
K_c forced convection evaporation constant
L latent heat of vaporization
$\dot{m}_v^{'''k}$ kth size evaporation rate per unit volume of that size group
$\dot{m}^{'''k}$ droplet mass transfer (as liquid phase) from the kth size group (to the $k-1$ group) per unit volume of the kth size group
n total number of droplets, $\Sigma_k \delta n^k$
N^k fractional number of droplets in the kth size group per unit size increment
p pressure
p' pressure correction
r radius/radial coordinate
T temperature
u axial mixture velocity
u_i mixture velocity in the i-direction
u_g axial gas velocity
u_{gi} gas velocity in the i-direction
u_l^k axial liquid velocity
u_{li}^k liquid velocity in the i-direction
u_{lgi}^k slip velocity in the i-direction, $u_{li}^k - u_{gi}$
x axial coordinate
x_i i-direction coordinate
Y mass fraction
$Y^{(l)}$ l-element mass fraction in each phase.

Greek symbols
α volume fraction
α, β exponents of the beta-function
Γ transport coefficient
δD^k droplet size increment of the kth size group
δn^k number of droplets in the kth size group
δ_{ij} Kronecker delta tensor
ε dissipation rate of k
λ thermal conductivity
μ dynamic viscosity
μ_t turbulent viscosity of the gas-phase
μ_{tl} turbulent liquid-phase viscosity
ν kinematic viscosity, μ/ρ
ρ density
σ Prandtl/Schmidt number
ϕ flow variable.

Subscripts
c centerline
e equilibrium
eff effective
g gas-phase or variance g
i, j, m i-, j-, m-direction
k turbulence kinetic energy
l liquid-phase
t turbulent
u zero evaporation
ε dissipation rate of k
0 free stream
1 injector exit.

Superscripts
$\bar{}$ time mean value
$\tilde{}$ density weighted (Favre-averaged) mean value ($\tilde{\phi} = \overline{\rho\phi}/\bar{\rho}$)
$'$ fluctuating component ($\phi' = \phi - \bar{\phi}$)
$''$ Favre fluctuating component ($\phi'' = \phi - \tilde{\phi}$)
k the kth size group 'fluid'
(l) element l.

phase and the kth dispersed liquid phase are given as follows,

$$\frac{\partial}{\partial x_i}(\bar{\rho}_g \bar{\alpha}_g \tilde{u}_{gi}) + \frac{\partial}{\partial x_i}(\bar{\rho}_g \overline{\alpha_g'' u_{gi}''}) = \sum_k \dot{m}_v^{'''k} \bar{\alpha}_l^k \quad (1)$$

$$\frac{\partial}{\partial x_i}(\bar{\rho}_l \bar{\alpha}_l^k \tilde{u}_{li}^k) + \frac{\partial}{\partial x_i}(\bar{\rho}_l \overline{\alpha_l'' u_{li}''}) = -\dot{m}_v^{'''k} \bar{\alpha}_l^k - \dot{m}^{'''k} \bar{\alpha}_l^k + \dot{m}^{'''k+1} \bar{\alpha}_l^{k+1}. \quad (2)$$

Similarly the momentum equations are,

$$\frac{\partial}{\partial x_i}(\bar{\rho}_g \bar{\alpha}_g \tilde{u}_{gi} \tilde{u}_{gj} - \bar{\alpha}_g \bar{\tau}_{gij} + \bar{\rho}_g \bar{\alpha}_g \overline{u_{gi}'' u_{gj}''} + \bar{\rho}_g \tilde{u}_{gj} \overline{\alpha_g'' u_{gi}''} + \bar{\rho}_g \tilde{u}_{gi} \overline{\alpha_g'' u_{gj}''}) = -(\bar{\alpha}_g'' + \bar{\alpha}_g) \frac{\partial \bar{p}}{\partial x_j} + \sum_k [f_D^k \bar{\alpha}_l^k (\tilde{u}_{lj}^k - \tilde{u}_{gj}) + \dot{m}_v^{'''k} (\bar{\alpha}_l^k \tilde{u}_{lj}^k + \overline{\alpha_l''^k u_{lj}''^k}) + f_D^k \bar{\alpha}_l^k (\overline{u_{lj}''^k} - \overline{u_{gj}''^k}) + f_D^k \overline{\alpha_l''^k (u_{lj}''^k - u_{gj}'')}] + \bar{\alpha}_g \bar{\rho}_g g_j \quad (3)$$

$$\frac{\partial}{\partial x_j}(\bar{\rho}_l\tilde{\alpha}_l^k\tilde{u}_{li}^k\tilde{u}_{lj}^k-\tilde{\alpha}_l^k\bar{\tau}_{lij}^k+\bar{\rho}_l\tilde{\alpha}_l^k\overline{u_{li}''^k u_{lj}''^k}+\bar{\rho}_l\tilde{u}_{lj}^k\overline{\alpha_l''^k u_{li}''^k}+\bar{\rho}_l\tilde{u}_{li}^k\overline{\alpha_l''^k u_{lj}''^k})$$
$$=-\tilde{\alpha}_l^k\frac{\partial\bar{p}}{\partial x_j}-f_D^k\tilde{\alpha}_l^k(\tilde{u}_{lj}^k-\tilde{u}_{gj})-(\dot{m}'''^k+\dot{m}_v'''^k)(\tilde{\alpha}_l^k\tilde{u}_{lj}^k+\overline{\alpha_l''^k u_{lj}''^k})$$
$$-f_D^k\tilde{\alpha}_l^k(\widetilde{u_{lj}''^k}-\widetilde{u_{gj}''})-\overline{f_D^k\alpha_l''^k(u_{lj}''^k-u_{gj}'')}$$
$$+\dot{m}'''^{k+1}(\tilde{\alpha}_l^{k+1}\tilde{u}_{lj}^{k+1}+\overline{\alpha_l''^{k+1}u_{lj}''^{k+1}})+\tilde{\alpha}_l\bar{\rho}_l g_j. \quad (4)$$

Finally, the global continuity must be included

$$\tilde{\alpha}_g+\overline{\alpha_g''}+\sum_k\tilde{\alpha}_l^k=1. \quad (5)$$

In the above equations, the subscripts 'g' and 'l' denote gas and liquid phases, respectively. $\tilde{u}_i$ is the density-weighted mean velocity in the i-direction and u_i'' is its fluctuating component. f_D is a momentum exchange coefficient; $\bar{p}$ is the mean pressure; g_j is the j-component of the gravitational acceleration; the superscript k denotes the kth droplet size group; $\dot{m}_v'''^k$, $\dot{m}'''^k$ and $\dot{m}'''^{k+1}$ are evaporation rate per unit volume of the kth size group, mass flowing out of the k-size group per unit volume of that size group and mass flowing into the k-size group from size group $(k+1)$ per unit volume of the $(k+1)$ group, respectively; α is volume fraction. τ_{ij} is the mean laminar stress tensor; for the gas phase, at high Reynolds number, only the main part of $\bar{\tau}_{ij}$, which is similar to the turbulent stress tensor, will be retained, namely

$$\bar{\tau}_{gij}\simeq\bar{\rho}_g\nu_g\left[\frac{\partial\tilde{u}_{gi}}{\partial x_j}+\frac{\partial\tilde{u}_{gj}}{\partial x_i}-(2/3)\frac{\partial\tilde{u}_{gm}}{\partial x_m}\delta_{ij}\right]. \quad (6)$$

A similar expression can be written for each liquid phase size group. However, the kinematic viscosity of the liquid phase is caused by the carrier phase molecular motion and hence should be replaced by ν_g [19]. The momentum exchange coefficient f_D^k is given by [13]

$$f_D^k=18Z\mu_g/(D^k)^2 \quad (7)$$

where D^k is a mean droplet diameter of the kth size group 'fluid' and μ_g is the gas laminar viscosity. Z may be calculated for deformable droplets [20] with evaporation effects [21] as

$$Z=[1+0.15\,Re_l^{0.687}+0.02\,Re_l/(1+42\,500/Re_l^{1.16})]/(1+B)^{0.25} \quad (8)$$

where B is the droplet transfer number and Re_l is the liquid droplet Reynolds number defined as

$$Re_l=\bar{\rho}_g D^k|\tilde{u}_{gj}-\tilde{u}_{lj}^k|/\mu_g. \quad (9)$$

In the equations above, only second-order correlation terms were retained [13]. Since the liquid phase density ρ_l is practically constant, the Favre and the time-averaging processes are identical, e.g.

$$\tilde{u}_l^k=\bar{u}_l^k \quad \text{and} \quad \overline{u_l''^k}=\overline{u_l'^k}=\overline{\alpha_l''^k}=\overline{\alpha_l'^k}=0.$$

In equation (3), $(\tilde{\alpha}_g''+\tilde{\alpha}_g)$ in the pressure gradient term can directly be obtained from equation (5) as $(1-\Sigma\tilde{\alpha}_l^k)$. It was found in the present paper, that the value of $\tilde{\alpha}_g''$ as can be obtained using the pdf and the state relationships for kerosene (to be introduced later), is much smaller than $\tilde{\alpha}_g$ for all possible values of $\tilde{f}$ and g. However, the value of $\tilde{\alpha}_g''$ is comparable to $\Sigma\tilde{\alpha}_l^k$ especially when $\Sigma\tilde{\alpha}_l^k$ is of the order of 10^{-5}. Therefore, $\tilde{\alpha}_g''$ may be neglected if it is only added to $\tilde{\alpha}_g$ but should be retained when $\tilde{\alpha}^k$ is involved as in equation (5).

THE TURBULENCE MODEL

The Reynolds stresses $(\overline{u_{gi}''u_{gj}''}$ and $\overline{u_{li}''^k u_{lj}''^k})$ are calculated by way of a two-phase k–ε model developed by Elghobashi and Abou-Arab [22] for constant-density flow and is extended here to variable-density flow. In this model, the concept of eddy diffusivity is invoked; hence:

$$-\overline{\bar{\rho}_g u_{gi}''u_{gj}''}=\nu_t\left[\frac{\partial\tilde{u}_{gi}}{\partial x_j}+\frac{\partial\tilde{u}_{gj}}{\partial x_i}-\frac{2}{3}\frac{\partial\tilde{u}_{gm}}{\partial x_m}\delta_{ij}\right]-\frac{2}{3}\tilde{k}\delta_{ij} \quad (10)$$

$$-\overline{\bar{\rho}_l u_{li}''^k u_{lj}''^k}=\frac{\nu_t}{\sigma_l^k}\left[\frac{\partial\tilde{u}_{li}^k}{\partial x_j}+\frac{\partial\tilde{u}_{lj}^k}{\partial x_i}-\frac{2}{3}\frac{\partial\tilde{u}_{lm}^k}{\partial x_m}\delta_{ij}\right]-\frac{2}{3}\tilde{k}_l\delta_{ij} \quad (10a)$$

where σ_l^k $(\equiv\nu_t/\nu_{tl}^k)$ is the liquid phase turbulent Schmidt number; its value for spray flames is expected to be higher than 1.0, reflecting the reduced effect of turbulent diffusion of the droplets relative to the gas phase. ν_t $(\equiv C_\mu\tilde{k}^2/\tilde{\varepsilon})$ and ν_{tl}^k are turbulent viscosities of gas and k-fluid. The last term in equations (10) and (10a) is small and can be neglected; it is shown merely to satisfy the balance conditions, $\overline{u_{gi}''u_{gi}''}=2\tilde{k}$ and $\overline{u_{li}''^k u_{li}''^k}=2\tilde{k}_l$. The gas turbulent kinematic viscosity ν_t is defined as

$$\nu_t=C_\mu\tilde{k}^2/\tilde{\varepsilon}. \quad (11)$$

The liquid phase Schmidt number σ_l^k can be calculated as [23]

$$\sigma_l^k=1+\tfrac{2}{3}\bar{\rho}_l\tilde{\varepsilon}/[C_\mu\tilde{k}f_D^k(1+\tilde{\alpha}_l^k\bar{\rho}_l/\bar{\rho}_g\tilde{\alpha}_g)]. \quad (12)$$

Here, $\tilde{k}$ is $(\overline{u_{gi}''u_{gi}''}/2)$ and $\tilde{\varepsilon}$ is its dissipation rate; C_μ is a constant of the model.

The density-weighted kinetic energy of turbulence $\tilde{k}$ and its dissipation rate $\tilde{\varepsilon}$ transport equations can be obtained from the instantaneous momentum equations of the carrier phase in a way similar to that of ref. [22],

$$\bar{\rho}_g\tilde{\alpha}_g\tilde{u}_{gi}\frac{\partial\tilde{k}}{\partial x_i}-\frac{\partial}{\partial x_i}\left[\left(\frac{\mu_t\tilde{\alpha}_g}{\sigma_k}\right)\frac{\partial\tilde{k}}{\partial x_i}\right]=\tilde{\alpha}_g(\tilde{G}+\tilde{\Delta}G)-\bar{\rho}_g\tilde{\alpha}_g(\tilde{\varepsilon}+\tilde{\Delta}\varepsilon) \quad (13)$$

$$\bar{\rho}_g\tilde{\alpha}_g\tilde{u}_{gj}\frac{\partial\tilde{\varepsilon}}{\partial x_j}-\frac{\partial}{\partial x_j}\left[\left(\frac{\mu_t\tilde{\alpha}_g}{\sigma_\varepsilon}\right)\frac{\partial\tilde{\varepsilon}}{\partial x_j}\right]=\tilde{\alpha}_g\left(\frac{\tilde{\varepsilon}}{\tilde{k}}\right)C_1(\tilde{G}+\tilde{\Delta}G)-\bar{\rho}_g\tilde{\alpha}_g\left(\frac{\tilde{\varepsilon}}{\tilde{k}}\right)(C_2\tilde{\varepsilon}+C_3\tilde{\Delta}\varepsilon) \quad (14)$$

where C_1, C_2, C_3 are further constants of the multiphase k–ε model while $\tilde{G}$ is a generation term. $\tilde{\Delta}G$ and $\tilde{\Delta}\varepsilon$ are additional generation and dissipation terms caused by α_g'', ρ_g', α_l'' and $\dot{m}_v'''$. They are modeled as

$$\tilde{\Delta}G=C_\alpha\frac{\tilde{k}}{\tilde{\varepsilon}}\frac{\mu_t}{\tilde{\alpha}_g\sigma_{\alpha g}}\frac{\partial\tilde{u}_{gi}}{\partial x_m}\left[\left(\frac{\partial\tilde{u}_{gi}}{\partial x_j}+\frac{\partial\tilde{u}_{gj}}{\partial x_i}\right)\frac{\partial(v_t\partial\tilde{\alpha}_g/\partial x_m)}{\partial x_j}+\left(\frac{\partial\tilde{u}_{gm}}{\partial x_j}+\frac{\partial\tilde{u}_{gj}}{\partial x_m}\right)\frac{\partial(v_t\partial\tilde{\alpha}_g/\partial x_i)}{\partial x_j}\right]+\frac{v_t}{\tilde{\alpha}_g\sigma_{\alpha g}}\frac{\partial\tilde{\alpha}_g}{\partial x_j}\frac{\partial\tilde{P}}{\partial x_j} \quad (15)$$

$$\tilde{\Delta}\varepsilon=\sum_k\left\{\frac{1}{\tilde{\alpha}_g\bar{\rho}_g}(\dot{m}_v^{\prime\prime\prime k}+\dot{m}_v^{\prime\prime\prime k})\left[(\tilde{u}_{li}^k-\tilde{u}_{gi})\frac{v_t}{\sigma_{\varepsilon l}^k\sigma_l^k}\frac{\partial\tilde{\alpha}_l^k}{\partial x_i}+\tilde{k}\left(1-\int_0^\infty\left(\frac{\Omega_1^k-\Omega_R^k}{\Omega_2^k}\right)E(\omega)\,d\omega\right)\times\left(\tilde{\alpha}_l^k+C_\phi\frac{\tilde{k}}{\tilde{\varepsilon}}\partial\left(\frac{v_t}{\sigma_l^k\sigma_{\varepsilon l}^k}\frac{\partial\tilde{\alpha}_l^k}{\partial x_m}\right)\Big/\partial x_m\right)+\tilde{\alpha}_l^k\frac{(\tilde{u}_{li}^k-\tilde{u}_{gi})}{\bar{\rho}_g^2\sigma_\rho}\mu_t\frac{\partial\bar{\rho}_g}{\partial x_i}\right]\right\}. \quad (16)$$

The above equations were obtained for high Reynolds numbers with pressure fluctuations and fourth order correlation terms ignored. C_ρ is a constant which is equal to 0.1 [24]; ω is the harmonic frequency of turbulence; $E(\omega)$ is the Lagrangian energy spectrum function of the carrier phase; Ω_1^k, Ω_2^k and R_R^k are functions of the carrier and dispersed phases properties, the droplet diameter and the harmonic frequency [24].

The Favre-averaging generating term $\tilde{G}$ is given, as for single phase, by

$$\tilde{G}=\mu_t\left(\frac{\partial\tilde{u}_{gi}}{\partial x_j}+\frac{\partial\tilde{u}_{gj}}{\partial x_i}\right)\frac{\partial\tilde{u}_{gi}}{\partial x_j}-\frac{2}{3}\frac{\partial\tilde{u}_{gm}}{\partial x_m}\left(\mu_t\frac{\partial\tilde{u}_{gm}}{\partial x_m}+\bar{\rho}_g\tilde{k}\right)-\mu_t\frac{\partial\bar{\rho}_g}{\partial x_m}\frac{\partial\tilde{P}}{\partial x_m}\Big/\bar{\rho}_g^2\sigma_\rho. \quad (17)$$

The last term in equations (16) and (17) is caused by the carrier phase density fluctuations. These two terms have nonzero values for reacting turbulent flows. The remaining correlation terms are modeled using the Boussinesq approximation [13]

$$-\overline{\alpha_g''u_{gi}''}=\left(\frac{v_t}{\sigma_{\alpha g}}\right)\frac{\partial\tilde{\alpha}_g}{\partial x_i};\quad -\overline{\alpha_g''^k u_{gi}''^k}=\left(\frac{v_t}{\sigma_{\varepsilon l}^k}\right)\frac{\partial\tilde{\alpha}_l^k}{\partial x_i} \quad (18)$$

$$-\overline{\alpha_l''^k u_{li}''^k}=\left(\frac{v_{li}^k}{\sigma_{\varepsilon l}^k}\right)\frac{\partial\tilde{\alpha}_l^k}{\partial x_i} \quad (19)$$

where $\sigma_{\alpha g}$ is a turbulent gas-phase Schmidt number. Similar expressions can be written for any flow variables. The terms involving u_{gi}'' result from the gas density fluctuations: u_{gi}'' is modeled as

$$u_{gi}''=-\rho_g'u_{gi}'/\bar{\rho}_g=(v_t/\rho_g\sigma_\rho)\partial\bar{\rho}_g/\partial x_i \quad (20)$$

where σ_ρ is a turbulent Schmidt number of the order of unity.

THE SPRAY MODEL

Modeling of spray flames is complicated by the fact that in addition to modeling the flow in the physical space we need also to model the variations in the droplet-size space, as indicated by Spalding [25]. Here, the droplet-size space is subdivided into a finite number of size groups. The kth size group (the kth 'fluid') is characterized by its mean droplet diameter D^k, its size increment δD^k and its number of droplets δn^k (or equivalently its volume fraction α_l^k). Within each size group ($D^k-\delta D^k/2$ to $D^k+\delta D^k/2$), the distribution is uniform, i.e. the number of droplets dn, corresponding to a small size increment dD ($dD\leqslant\delta D^k$), is given by

$$dn=(\delta n^k/\delta D^k)\,dD. \quad (21)$$

The conservation equations (equations (2) and (4)) for the kth fluid (size group) are affected by the evaporation rate $\dot{m}_v'''^k$, the rate of mass flowing out (in droplet-size space) of the k size group $\dot{m}'''^k$ and inflow of mass from the $(k+1)$ size group $\dot{m}'''^{k+1}$ due to the decrease in droplet diameter. The rate of change of droplet diameter (dD/dt), which influences directly $\dot{m}_v'''^k$, $\dot{m}'''^k$ and $\dot{m}'''^{k+1}$, can be calculated as follows [25]:

$$dD/dt=-K_c/2D. \quad (22)$$

Here K_c is the forced-convection evaporation constant [21]

$$K_c=[1+0.269\,Re^{0.581}\,Pr^{0.333}]\times\frac{8}{\rho_l}\Gamma[\ln(1+B)]/(1+B)^{0.67} \quad (23)$$

where Pr is the gas phase film Prandtl number; the exchange coefficient Γ is λ_g/C_{p_g} ($\equiv\mu_g/Pr$); the transfer number B is $C_{p_v}(T-T_{l,sat})/L_l$; λ_g and C_{p_v} are the gas phase thermal conductivity and constant pressure specific heat of the fuel vapor respectively; T is the gas temperature; T_l and L_l are the droplet temperature and latent heat of vaporization, respectively. The heating up period is neglected in the present study as most hydrocarbon fuels start to evaporate near room temperature even inside the atomizer. Equation (22) is used to obtain the evaporation rate per unit volume of the kth size group, from that size group as

$$\dot{m}_v'''^k=3K_c\rho_c/2(D^k)^2. \quad (24)$$

At the smaller-size boundary ($D=D^k-\delta D^k/2$), the number of droplets leaving the kth size group per unit time is calculated using equations (21) and (22) as

$$\left|\frac{dn}{dt}\right|^k=(\delta n^k/\delta D^k)/[K_c/2(D^k-\delta D^k/2)]. \quad (25)$$

The droplets leaving the kth size group have a diam-

eter of $(D^k-\delta D^k/2)$; therefore, the mass of droplets leaving the kth size group per unit time and volume of that group is

$$\dot{m}'''^k = [(D^k-\delta D^k/2)/D^k]^2 K_e \rho_l / 2D^k \delta D^k. \quad (26)$$

Equation (26) can also be used to calculate $\dot{m}'''^{k+1}$, the inflow of droplets from $k+1$ to k size groups, if k is replaced by $k+1$. It is noted that the smallest size group loses no mass at its zero diameter boundary (see equation (26)) when $D^k = \delta D^k/2$ for $k = 1$; this size group loses mass only by evaporation.

The fractional number of droplets per size increment N^k $(\equiv \delta n^k/(n\delta D^k))$ can be related to the corresponding volume fraction $\tilde{\alpha}_l^k$ $(=\bar{\alpha}_l^k)$, of the kth size group, by the following two relations:

$$N^k = \frac{\bar{\alpha}_l^k/(D^k)^3}{\left(\sum_k [\alpha_l^k/(D^k)^3]\right)\delta D^k} \quad (27)$$

$$\tilde{\alpha}_l^k = \frac{(1-\tilde{\alpha}_g)(D^k)^3 N^k \delta D^k}{\sum_k [(D^k)^3 N^k \delta D^k]} \quad (28)$$

where n $(\equiv \Sigma n^k)$ is the total number of droplets.

Equation (27) is needed to transfer liquid volume fractions into the number of droplets while equation (28) is needed for the reverse process.

Evaporation variable

Due to the finite evaporation rate equation (24), the mean mass fraction of the liquid phase

$$\tilde{Y}_l\left(\equiv \sum_k \tilde{Y}_l^k,\ \tilde{Y}_l^k = \bar{\alpha}_l^k \bar{\rho}_l^k \Big/ \left(\sum_k \bar{\rho}_l^k \bar{\alpha}_l^k + \tilde{\alpha}_g \bar{\rho}_g\right)\right)$$

in the reacting spray, will generally be higher than the corresponding value $\tilde{Y}_{l,e}$ if phase equilibrium is assumed. Therefore, a mean evaporation variable $\tilde{e}$ $(\simeq \tilde{e}$, since ρ_l is assumed constant) can be defined as

$$\tilde{e} = (\tilde{Y}_{l,u} - \tilde{Y}_l)/(\tilde{Y}_{l,u} - \tilde{Y}_{l,e}) \quad (29)$$

where $\tilde{Y}_{l,u}$ is the mean mass fraction of the liquid phase with no evaporation $(\tilde{e} = 0)$; in this case, $\tilde{Y}_{l,u} = f$.

THE COMBUSTION MODEL

Fast chemistry is assumed so that the reacting mixture is in chemical equilibrium. However, finite evaporation rate (phase nonequilibrium) is considered. The evaporation variable e introduced above is a measure of the departure from phase equilibrium. Therefore, the instantaneous state relationship is a function of a multi-phase mixture fraction f and the evaporation variable e. Any scalar except ϕ is evaluated from

$$\tilde{\phi} = \int_0^1 \int_0^1 \phi(f,e)\tilde{P}(f)\tilde{P}(e)\,df\,de \quad (30)$$

where $\tilde{P}(e)$ is determined from e as follows:

$$\tilde{P}(e) = (1-\tilde{e})\delta(e) + \tilde{e}\delta(1-e) \quad (31)$$

and $\tilde{P}(f)$ is the Favre probability density function which may be characterized by $\tilde{f}$ and g $(\equiv \widetilde{f''f''})$. Consequently,

$$\tilde{\phi} = \int_0^1 \phi(f,\tilde{e})\tilde{P}(f)\,df \quad (32)$$

in which $\phi(f, \tilde{e})$ is the instantaneous ϕ at an $e = \tilde{e}$ plane,

$$\phi(f,\tilde{e}) = (1-\tilde{e})\phi(f,0) + \tilde{e}\phi(f,1) \quad (33)$$

where $\phi(f, 0)$ is to be calculated from state relationships with no evaporation $(e = 0)$ while $\phi(f, 1)$ is related to f through full thermodynamic equilibrium state relationships $(e = 1)$.

The time mean mixture density $\bar{\rho}$ can be calculated from,

$$\bar{\rho} = \left[\int_0^1 \frac{1}{\rho(f,\tilde{e})}\tilde{P}(f)\,df\right]^{-1}. \quad (34)$$

The Favre pdf $\tilde{P}(f)$ is related to the time-averaging pdf $P(f)$ as

$$P(f) = \bar{\rho}\tilde{P}(f)/\rho \quad (35)$$

which is used to calculate the Favre carrier phase pdf,

$$\tilde{P}_g(f) = \rho_g P(f) \Big/ \int_0^1 \rho_g(f,\tilde{e})P(f)\,df. \quad (36)$$

For the liquid phase, the Favre and time-averaging pdf's are identical since ρ_l is constant. $\bar{\alpha}_g''$, which appear in equations (3)–(5), can be calculated using the above pdf's

$$\overline{\alpha_g''} = \int_0^1 \alpha_g(f,\tilde{e})[P(f) - \tilde{P}_g(f)]\,df \quad (37)$$

where $\alpha_g(f, \tilde{e})$ can be obtained from the state relationships explained above.

Multi-phase mixture fraction

An exact instantaneous mixture fraction conservation equation can be derived from the instantaneous conservation equations for mass and any reacting element (l) [12]. For the multiphase mixture, it is

$$\frac{\partial}{\partial t}(\rho f) + \frac{\partial}{\partial x_i}\left(\rho u_i f - \Gamma_f \frac{\partial f}{\partial x_i}\right) + \frac{\partial}{\partial x_i}\sum_k \left[\rho_l \alpha_l^k u_{lgi}^k (f_l - f) - \rho_l \alpha_l^k \gamma_{lg} \frac{\partial}{\partial x_i}(f_l - f)\right] + \frac{\partial}{\partial x_i}\left[\Gamma_g \alpha_g (f_l - f)\frac{\partial L^k}{\partial x_i}\right] = 0 \quad (38)$$

where Γ_f $(\equiv(\alpha_g\mu_g + \alpha_l\mu_l)/Sc)$ is a mixture diffusion coefficient;

$$\rho \left(\equiv \rho_g \alpha_g + \sum_k \rho_l \alpha_l^k \right)$$

is the mixture density:

$$u_i \left(\equiv \left[\rho_g \alpha_g u_{gi} + \sum_k \rho_l \alpha_l^k u_{li}^k \right] \Big/ \rho \right)$$

is the mixture velocity; f_l is a mixture ratio of the liquid phase ($=1.0$ for spray flames); u_{lgi}^k is the kth size group slip velocity in the i-direction; γ_{lg} is a 'slip' diffusivity; L^k is a loading ratio [12].

Equation (38) is used to derive the final form of the steady-state, Favre-averaged, 'multi-phase mixture fraction' transport equation as,

$$\frac{\partial}{\partial X_i}\left(\bar{\rho}\tilde{u}_i\tilde{f} - \Gamma_{f,\mathrm{eff}}\frac{\partial \tilde{f}}{\partial X_i}\right) + \frac{\partial}{\partial X_i}\sum_k \left[\bar{\rho}_l \tilde{\alpha}_l^k \tilde{u}_{lgi}^k (\tilde{f}_l - \tilde{f}) - \bar{\rho}_l \tilde{\alpha}_l^k \gamma_{lg,\mathrm{eff}} \frac{\partial}{\partial X_i}(\tilde{f}_l - \tilde{f}) + \bar{\rho}_l \alpha_l''^k u_{lgi}''^k (\tilde{f}_l - \tilde{f}) - \bar{\rho}_l \tilde{u}_{lgi}^k \alpha_l''^k f''\right] = 0. \quad (39)$$

$\bar{\rho}_l \alpha_l''^k u_{lgi}''^k$ is modeled, using equation (18), as

$$\bar{\rho}_l \alpha_l''^k (u_{li}''^k - u_{gi}'') = -\bar{\rho}_l \gamma_{lg,t} \frac{\partial \tilde{\alpha}_l^k}{\partial X_i} \quad (40)$$

while

$$\sum_k [\bar{\rho}_l \tilde{u}_{lgi}^k \alpha_l''^k f'']$$

is modeled, using the pdf relationships (equations (30)–(33)), as

$$\sum_k \bar{\rho}_l \tilde{u}_{lgi}^k \alpha_l''^k f'' \simeq \bar{\rho}_l \left(\sum_l^{k_{cl}} \tilde{u}_{lgi}^k / k_{cl} \right) \times \int_0^1 [(1-\tilde{e})(\alpha_l(f,0) - \tilde{\alpha}_l) + \tilde{e}(\alpha_l(f,1) - \tilde{\alpha}_l)](f - \tilde{f}) P(f)\, \mathrm{d}f \quad (41)$$

where $\alpha_l(f,0)$ and $\alpha_l(f,1)$ are from the state relationship planes at $e = 0$ and 1 respectively.

$$\tilde{\alpha}_l \left(= \sum_k \tilde{\alpha}_l^k \right) \quad \text{and} \quad \alpha_l'' \left(\equiv \sum_k \alpha_l''^k \right)$$

are the mean cumulative volume fraction of the liquid phase and its fluctuating component.

In equation (39) $\Gamma_{f,\mathrm{eff}}$ and $\gamma_{lg,\mathrm{eff}}$ are effective exchange coefficients,

$$\Gamma_{f,\mathrm{eff}} = \Gamma_f + \left[\left(\sum_k \tilde{\alpha}_l^k / \sigma_l^k \right) + \tilde{\alpha}_g \right] \mu_t / \sigma_f \quad (42)$$

$$\gamma_{lg,\mathrm{eff}} = \gamma_{lg} + [v_{tl}^k - v_t]/\sigma_f \quad (43)$$

where σ_f is a turbulent Schmidt number of order unity.

Multi-phase mixture fraction fluctuations

The transport equation of mean square fluctuations of the mixture fraction of two-phase reacting flows can be derived from equation (38). This is done by multiplying equation (38) by f'', then performing time-averaging on the resulting equation to yield $\tilde{g}$ ($\equiv \widetilde{f''f''}$) as follows:

$$\frac{\partial}{\partial X_i}\left[\bar{\rho}\tilde{u}_i\tilde{g} - \Gamma_{g,\mathrm{eff}}\frac{\partial \tilde{g}}{\partial X_i}\right] = C_{g1}\mu_t \left[\left(\frac{\partial \tilde{f}}{\partial X_i}\right)^2 + \sum_k \bar{\rho}_l \tilde{\alpha}_l^k \left(\frac{1}{\bar{\rho}_l \sigma_l^k} - \frac{1}{\bar{\rho}_g}\right) \frac{\partial \tilde{f}}{\partial X_i}\frac{\partial}{\partial X_i}(\tilde{f}_l - \tilde{f}) \right] + \Delta G_g + \sum_k \left[\bar{\rho}_l \tilde{\alpha}_l^k \tilde{u}_{lgi}^k \frac{\partial \tilde{g}}{\partial X_i} - \frac{\partial}{\partial X_i}\left(\bar{\rho}_l \tilde{\alpha}_l^k \gamma_{lg,g} \frac{\partial \tilde{g}}{\partial X_i}\right) \right] - C_{g2}\bar{\rho}\tilde{g}\tilde{\varepsilon}/\tilde{k} \quad (44)$$

where C_{g1} and C_{g2} are constants of the model of order $2/\sigma_f$ and 2.0. $\Gamma_{g,\mathrm{eff}}$ and $\gamma_{lg,g}$ are effective exchange coefficients

$$\Gamma_{g,\mathrm{eff}} = (\tilde{\alpha}_g \mu_g + \tilde{\alpha}_l \mu_l)/Sc + \left(\tilde{\alpha}_g + \sum_k \frac{\tilde{\alpha}_l^k}{\sigma_l^k} \right) \mu_t / \sigma_g \quad (45)$$

$$\gamma_{lg,g} = \gamma_{lg} + [v_{tl}^k - v_t]/\sigma_g \quad (46)$$

where σ_g is a turbulent Schmidt number, similar to the case of reacting single-phase flow [16].

ΔG_g is an extra generation/dissipation term caused by volume fraction fluctuations and is given as

$$\Delta G_g \simeq \frac{\partial}{\partial X_i}[\bar{\rho}_l \langle \tilde{u}_{lgi}^k \rangle_k (\tilde{f}_l - \tilde{f})] f'' \alpha_l'' + \bar{\rho}_l \langle \tilde{u}_{lgi}^k \rangle_k (\tilde{f}_l - \tilde{f}) \frac{\partial \tilde{f}}{\partial X_i} f'' \frac{\partial \alpha_l''}{\partial f} \quad (47)$$

where $\langle \ldots \rangle_k$ is the mean value over all size groups. $\widetilde{f''\alpha_l''}$ is calculated as in equation (41) while $(\widetilde{f''\partial \alpha_l''/\partial f})$ is calculated from a similar expression.

The probability density function

Different shapes of pdf's have been used in the modeling of turbulent diffusion flames. Clipped Gaussian pdf without intermittency [7–9, 26, 27] and with intermittency [28] have been used. The beta-function has recently been used as another alternative for the shape for the pdf as it is appropriately bound between zero and one [29, 30].

In the present work, a beta-function pdf is used which is defined by the following equation:

$$\tilde{P}(f) = f^{\alpha-1}(1-f)^{\beta-1} \Big/ \int_0^1 f^{\alpha-1}(1-f)^{\beta-1}\, \mathrm{d}f. \quad (48)$$

The exponents α and β can be related to the mean mixture fraction $\tilde{f}$ and its variance $\tilde{g}$ by

$$\alpha = \tilde{f}\left[\frac{\tilde{f}(1-\tilde{f})}{\tilde{g}} - 1 \right] \quad (49)$$

$$\beta = (1-\tilde{f})\left[\frac{\tilde{f}(1-\tilde{f})}{\tilde{g}} - 1\right]. \quad (50)$$

The values of $\tilde{f}$ and $\tilde{g}$ are to be computed from their transport equations.

The model constants used are: $C_\mu = 0.09$, $C_1 = 1.44$, $C_2 = 1.84$, $C_3 = 1.2$, $C_{g1} = 2.8$, $C_{g2} = 1.84$, $\sigma_l^k =$ equation (12), $\sigma_k = 1.0$, $\sigma_\varepsilon = 1.3$, $\sigma_f = \sigma_g = S_c = 0.7$, $C_\alpha = 0.1$, $\alpha_{\alpha l} = \sigma_{\alpha g} = \sigma_\rho = 1.0$, most of which are the standard values.

State relationships

The present multi-fluid model is used to predict the kerosene spray flame of Onuma and Ogasawara [18]. The corresponding equilibrium state relationships for combusting kerosene spray in atmospheric air, with phase equilibrium ($e = 1$), are depicted in Fig. 1. A complete description of the equilibrium computational algorithm, which is based on the Gibbs free energy minimization approach, is given in refs. [3, 7–9].

The gas and liquid phase mass fractions (Y_g and Y_l) are linearly related to f in the case of state relationships with no evaporation and chemical reaction, i.e. when $e = 0$. Constant $\tilde{e}$ planes ($0 < \tilde{e} < 1.0$) can be constructed, for nonequilibrium state relationships, as described by equation (33).

EXPERIMENTAL DATA AND BOUNDARY CONDITIONS

A good number of data sets for combusting spray flames exist [4, 18]. The validation of the present multi-fluid reacting model to the data of ref. [18], an upwardly directed co-flowing air jet–kerosene spray flame, is presented here. The Reynolds number for this flame was 24 000 [18]. The air atomizing injector outlet diameter was 2 mm. Liquid phase and gas phase mean velocities, ($\tilde{u}_{l1}^k$, $\tilde{u}_{g1}$) were estimated as 15 and 80 m s^{-1}. The loading ratio ($\equiv \bar{\rho}_l \tilde{\alpha}_l / \bar{\rho}_g \tilde{\alpha}_g$) at the injector exit was 8.8. The co-flowing air velocity ($\tilde{u}_{g0}$) was 8.5 m s^{-1}. The measured droplet-size distribution, in the non-burning kerosene spray, is discretized into five size groups with mean diameters (D^k) equal to 10, 30, 50, 70 and 90 μm and size increment (δD^k) of 20 μm.

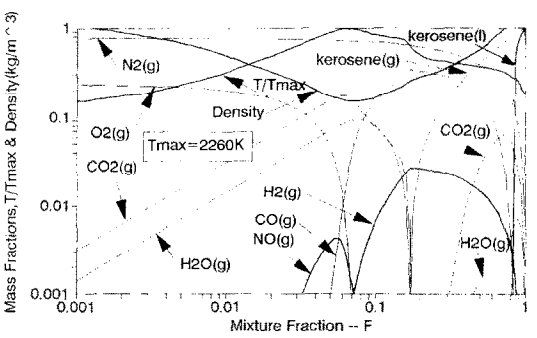

FIG. 1. Equilibrium state relationships for kerosene burning in air at atmospheric pressure ($e = 1.0$ and $T_{max} = 2290$ K).

The values of fractional number of droplets per size increment $N^k \times 10^3$ are 34, 9.5, 3.5, 2.0 and 1.0 μm^{-1} for $k = 1$, 2, 3, 4 and 5. The corresponding liquid phase volume fractions at nozzle exit $\tilde{\alpha}_l^k$ ($k = 1, 2, \ldots, 5$) can be calculated directly from the above information and equation (28), while $\tilde{\alpha}_{l0}^k$ of the co-flowing stream is equal to zero. The initial turbulence intensity ($(2k/\varepsilon)^{1/2}/\tilde{u}_{g0}$) is taken to be about 5% while the turbulent length scale ($c_\mu^{3/4} k^{3/4}/\varepsilon$) is taken as 3% of the injector radius [30]. The effect of the assumed turbulence intensity rapidly diminishes downstream of the injector [30].

SOLUTION PROCEDURE

The solution procedure is based mainly on an iterative-marching integration algorithm as described in refs. [13, 31]. The main dependent variables are $\tilde{u}_{gi}$, $\tilde{u}_{li}^k$, p', $\tilde{k}$, $\tilde{\varepsilon}$, $\tilde{f}$, $\tilde{g}$ and $\tilde{\alpha}_l^k$, where p' is a 'pressure correction'. $\tilde{u}_{gi}$ and $\tilde{u}_{li}^k$ are computed from equations (3) and (4). p' is computed from a combined equation derived from equations (1) and (2). The remaining variables $\tilde{k}$, $\tilde{\varepsilon}$, $\tilde{f}$, $\tilde{g}$ and $\tilde{\alpha}_l^k$ are to be computed from equations (13), (14), (39)–(44) and (2). The solution domain is overlaid with a non-uniform 2D axisymmetric grid. Since the obtained difference equations are nonlinear and coupled, few iterations are performed at each cross-stream plane, until the error in each equation is less than 1%, before marching downstream to the next plane. The present predictions for combusting kerosene spray were computed using 600 (axial) grid nodes $\times 40$ radial nodes, covering an axial distance of 200 jet diameters. The axial grid lines were made to spread out radially in proportion to the jet spreading rate as one marches downstream. The above grid gave nearly grid independent results.

RESULTS AND DISCUSSION

The predicted axial mean profiles of the centerline gas temperature $\tilde{T}$, gas-phase axial velocity $\tilde{u}_g$ and liquid-phase axial velocities for the first and fifth size groups ($\tilde{u}_l^k$, $k = 1$ and 5) are depicted in Fig. 2; the corresponding experimental data [18] for $\tilde{T}$ and $\tilde{u}_g$ are also shown. The agreement between predictions and measurements for $\tilde{T}$ and $\tilde{u}_g$ is fairly good for the whole spray flame length. $\tilde{u}_g$ is underpredicted for the whole flame length, which is a general feature of the parabolic k–ε model [32]. On the other hand, the axial gas temperature is underpredicted for $x/d < 40$ followed by overprediction of $\tilde{T}$ for $x/d > 50$. The maximum overprediction of $\tilde{T}$ occurs near stoichiometric conditions (maximum T) which may be attributed to soot/droplets deposition on the measuring thermocouple, flame radiation, or to finite chemical kinetic effects. As the liquid-phase injected velocity is much lower than the corresponding gas velocity, the first and fifth size-group velocities ($\tilde{u}_l^k$, $k = 1$ and 5) respond to the gas velocity and increase reaching maximum values before they start to decrease. The

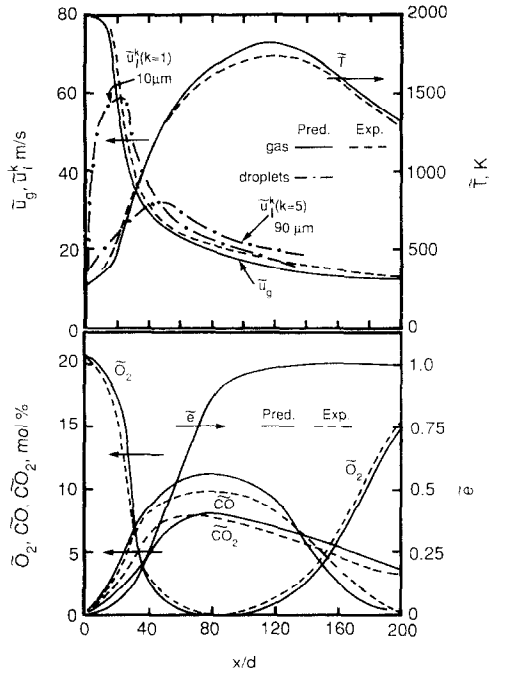

FIG. 2. Axial variation of mean centerline gas temperature, gas axial velocity and liquid phase first and fifth size-group axial velocities, species concentrations, evaporation variable in the kerosene spray flame.

response of the 10 μm group ($k = 1$) is much faster than the 90 μm group ($k = 5$), as shown in Fig. 2.

Figure 2 also shows the axial profiles of the evaporation variable $\tilde{e}$ and the mole fractions of O_2, CO and CO_2 together with the corresponding experimental data [18] for the kerosene spray flame. The oxygen mole fraction is slightly overpredicted near the injector and is somewhat underpredicted for $x/d > 40$ indicating a slow chemical reaction near the injector and a reverse tendency further downstream. The CO and CO_2 profiles are also well predicted with a maximum error of about ± 2 molar %. The $\tilde{e}$ axial profile shows that for $x/d < 100$ the liquid kerosene and its vapor are in a nonequilibrium phase state, as shown in Fig. 2. The $\tilde{e}$ profile exhibits a fast increase for x/d ranging between 60 and 80. Experimental data are needed to verify the trend of the evaporation variable axial profile.

The radial profiles, at $x/d = 100$, of the gas temperature and axial velocity, together with the corresponding experimental data [18] are illustrated in Fig. 3. Here the measured profiles show nonsymmetrical behavior with the peak values shifted to the left. The main differences between the predictions and the measurements result from this nonsymmetrical behavior. For $r/x > -0.07$, $\tilde{T}$ is overpredicted while for r/x ranging between -0.07 and -0.2 it is underpredicted. The gas axial velocity $\tilde{u}_g$ is in good agreement for all values of r/x except when $|r/x|$ is less than 0.05. The liquid phase axial velocity of the 90 μm size group ($k = 5$) is higher than the 10 μm size-group axial velocity at $x/d = 100$, as can be seen from Fig. 3. The slip velocity of the first size group is negligible while for the fifth size group the maximum slip velocity ($\tilde{u}_{lg}^k$, $k = 5$) is about 10% of the $\tilde{u}_g$.

Figure 3 also depicts the radial profiles of the chemical species concentrations, at $x/d = 100$, for the prediction and the experimental data [18]. The main differences between them again result from the nonsymmetrical nature of the experimental data. In the central part of the flame the O_2 concentration is underpredicted which is consistent with the overprediction of CO and CO_2 concentrations and the gas temperature.

The predicted and measured [18] droplet-size distribution vs droplet diameter at the centerline of the kerosene spray flame, at $x/d = 75$, are shown in Fig. 4. The fractional number of droplets of each size group per unit size increment N^k ($\equiv \delta n^k/(n\delta D^k)$) was computed from the computed values of $\tilde{\alpha}_l^k$, using equation (27). The number of droplets of the first size group has dropped to less than one-half of its value at the injector exit plane. This could be explained on the basis of the high evaporation rate and turbulent diffusion compared to the larger size groups ($k \geq 2$). However, the increase of N^k of the second and third size groups, relative to injector exit plane values, is attributed to droplet transfer from larger size groups.

The above confirms the validity of the proposed multiphase density-weighted reacting model. Since the model is equally applicable to submerged combustion, the model has been used to predict the flame like

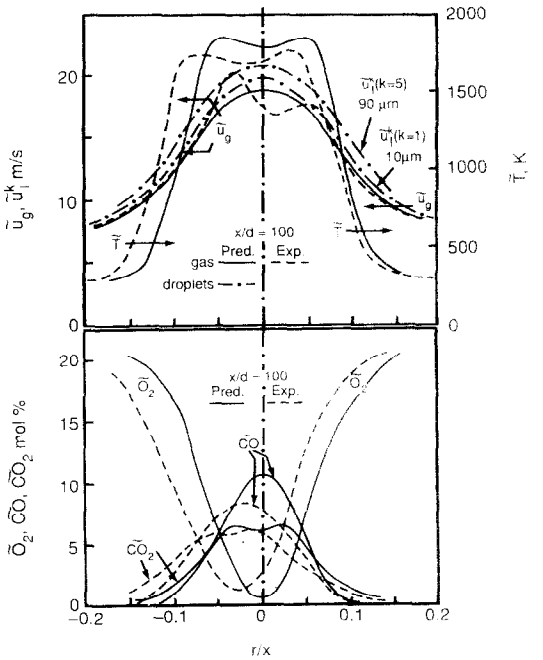

FIG. 3. Radial profiles of gas temperature, axial velocities of the gas and liquid phases (10 μm and 90 μm droplets-size groups), and chemical species concentrations at $x/d = 100$.

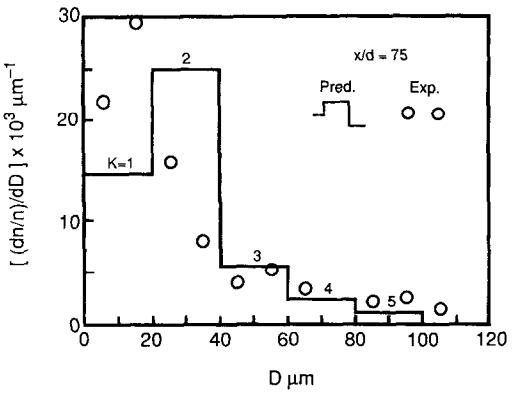

FIG. 4. Droplet size distribution at the axis of the kerosene spray flame at $x/d = 75$.

structure of a liquid metal combustion [33]. The latter involves the reaction of a turbulent gaseous SF_6 jet submerged in a lithium liquid bath as in the design of the SCEPS for undersea propulsion [34].

CONCLUSION

The proposed multi-fluid combustion model presents new transport equations for the mean mixture fraction and its variance of multi-phase reacting flows, in addition to a new 'evaporation variable', e, essential for modeling spray flames. The evaporation variable and the new transport equations for $\tilde{f}$ and $\tilde{g}$ are equally applicable to any reacting multi-phase systems such as liquid metal fuel combustors. The present reacting multi-fluid model has been used to predict a kerosene spray flame for which experimental data exists. The obtained level of agreement between predictions and corresponding experimental data confirms the validity of the model proposed and its possible use to predict other multiphase flames including the submerged liquid metal combustion.

Acknowledgement—The research was sponsored by the U.S. Office of Naval Research, under the technical management of Dr G. Roy.

REFERENCES

1. M. M. M. Abou-Ellail and E. E. Khalil, A mathematical model of gas–liquid interaction in the turbulent reacting flows, *J. Appl. Math. Modelling* **4**, 136–138 (1980).
2. M. M. M. Abou-Ellail and M. M. El-Koth, Description and validation of a prediction procedure for diesel engine swirl chamber two-phase flows, *Proc. 3rd International Conference on Numerical Methods in Laminar and Turbulent Flow*, Seattle, pp. 1224–1237 (1983).
3. S. H. Chan, Y. G. Zhao, P. J. Janke and C. C. Tan, Combustion of turbulent gaseous fluorine jets submerged in molten lithium fuel, *AIAA/ASME Thermophysics and Heat Transfer Conference*, Seattle, WA (1990).
4. E. E. Khalil and J. H. Whitelaw, Aerodynamic and thermodynamic characteristics of kerosene-spray flames, *Sixteenth Symposium (International) on Combustion*, The Combustion Institute, pp. 569–576 (1976).
5. L. D. Chen and G. M. Faeth, Structure of turbulent reacting gas jets submerged in liquid metals, *Combust. Sci. Technol.* **11**, 111–131 (1983).
6. T. F. Lin, Modelings of submerged liquid metal combustion, *27th JANAF Combustion Subcommittee Meeting* Vol. 3, pp. 577–586 (1990).
7. S. H. Chan, C. C. Tan, Y. G. Zhao and P. J. Janke, Li–SF_6 combustion in stored chemical energy propulsion system, *Twenty-third Symposium (International) on Combustion*, The Combustion Institute, pp. 1139–1146 (1990).
8. S. H. Chan, P. J. Janke and T. R. Shen, Equilibrium computations of multiphase nonideal electrolytic systems and structure of turbulent reacting dissolving jets, *Twenty-second Symposium (International) on Combustion*, The Combustion Institute, pp. 721–729 (1988).
9. S. H. Chan and T. R. Shen, Turbulent reacting gas jets in liquids at elevated temperatures and pressures, *Combustion and Fires* (Edited by R. K. Shah), pp. 455–460. ASME (1989).
10. D. B. Spalding, A general-purpose computer program for multi-dimensional one- and two-phase flow, *J. Mathematics and Computers in Simulation* **XXIII**, 267–276 (1981).
11. D. B. Spalding, The two-fluid model of turbulence applied to combustion phenomena, *AIAA J.* **24**(6), 876–884 (1986).
12. S. H. Chan and M. M. M. Abou-Ellail, A reacting two-fluid model for turbulent diffusion flames, *3rd ASME-JSME Thermal Engineering Proceedings*, Vol. 5, Reno, Nevada, pp. 95–103 (1991).
13. M. M. M. Abou-Ellail and T. W. Abou-Arab, Prediction of two-phase flow and heat transfer in vertical pipes, *Proc. 5th Symposium on Turbulent Shear Flows*, Ithaca, N.Y., pp. 8.1–8.7 (1985).
14. A. D. Gosman, E. Ioannides, D. A. Lever and K. A. Cliffe, A comparison of continuum and discrete droplet finite-difference models used in the calculation of spray combustion in swirling turbulent flows, AERE Harwell Report TP865 (1980).
15. A. D. Gosman and E. Ioannides, Aspects of computer simulation of liquid-fueled combustors, AIAA Paper No. 81-0323 (1981).
16. D. B. Spalding, Concentration fluctuations in a round turbulent jet, *Chem. Engng Sci. J.* **26**, 95–107 (1971).
17. L. A. Parnell, J. T. Gilchrist and D. J. Rogerson, Flash and real-time radiographic study of closed liquid metal combustion, *2nd ONR Propulsion Meeting*, Irvine, CA, pp. 188–205 (1989).
18. Y. Onuma and M. Ogasawara, Studies of the structure of a spray combustion flame, *Fifteenth Symposium (International) on Combustion*, The Combustion Institute, pp. 453–465 (1974).
19. M. A. Rizk and S. E. Elghobashi, A two-equation turbulence model for dispersed dilute confined two-phase flows, *Int. J. Multiphase Flow* **15**(1), 119–133 (1989).
20. N. C. Markatos and A. K. Singhal, Numerical analysis of one-dimensional two-phase flow in a vertical cylindrical passage, *J. Adv. Engng Software* **4**(3), 99–106 (1983).
21. W. A. Sirignano, Heat and mass transfer in liquid–gas spray systems, presented at the *1990 ASME Winter Annual Meeting*, Dallas, TX (1990).
22. S. E. Elghobashi and T. W. Abou-Arab, Two equation turbulence model for two-phase flows, *J. Phys. Fluids* **26**(4), 931–938 (1982).
23. O. Siminin and P. L. Viollet, Numerical modelling of devolatilization in pulverized coal injection inside a hot coflowing air flow, *Lecture Notes in Engineering (Turbulent Reacting Flows)* **40**, 824–846 (1989).
24. A. A. Mostafa and S. E. Elghobashi, Effect of liquid droplets on turbulence in a round gaseous jet, NASA Contractor Report-175063 (1986).

25. D. B. Spalding, The calculation of combustion processes, Lecture Notes, Imperial College, London, RF/TN/A/3 (1971).
26. F. C. Lockwood and A. S. Naguib, The prediction of the fluctuations in the properties of free, round-jet, turbulent diffusion flames, *Combust. Flame* **24,** 109–124 (1975).
27. M. M. M. Abou-Ellail, A. D. Gosman, F. C. Lockwood and I. E. A. Megahed, Description and validation of a three-dimensional procedure for combustion chamber flows, *Turbulent Combustion* (Edited by L. A. Kennedy), Progress in Astronautics and Aeronautics **58,** 163–190 (1978).
28. J. H. Kent and R. W. Bilger, The prediction of turbulent diffusion flame fields and nitric oxide formation, *Sixteenth Symposium (International) on Combustion*, The Combustion Institute, pp. 1643–1656 (1976).
29. S. M. Correa, M. C. Drake, R. W. Pitz and W. Shyy, Prediction and measurement of a non-equilibrium turbulent diffusion flame, *Twentieth Symposium (International) on Combustion*, The Combustion Institute, Vol. 35, pp. 337–343 (1984).
30. M. M. M. Abou-Ellail and H. Salem, A skewed PDF-combustion model for jet diffusion flames, *J. Heat Transfer* **112,** 1002–1007 (1990).
31. H. A. Warda and M. M. M. Abou-Ellail, Computer simulation of two-phase flow in oil wells using gas-lift, *Engineering Software for Microcomputers, Proceedings 1st International Conference*, Venice, pp. 567–581 (1984).
32. F. C. Lockwood and P. Stolakis, Assessment of two turbulent models for turbulent round diffusion jet with combustion, *4th Symposium Turbulent Shear Flows*, pp. 10.25–10.31 (1983).
33. S. H. Chan, Multiphase turbulent liquid metal fuel combustion, *Progress in Energy and Combustion Science—An International Review Journal* (in press).
34. S. H. Chan and M. M. M. Abou-Ellail, A multi-fluid model of turbulence for Li SF_6 submerged combustion, *AIAA J.* **31**(8), 1526–1529 (1993).